Head-disk Spacing Control for an Advanced Rotary Tester

Xinghui Huang, Nils Gokemeijer, Mark Bedillion, and Patrick Chu

Abstract— This paper discusses head-disk spacing (HDS) control for an advanced rotary tester (ART). With active control of HDS, the ART enables testing of individual recording head sliders and evaluation of novel magnetic recording processes with great flexibility. In this paper, system characterization and servo control design for the ART are presented. Various hardware and design issues are addressed and the corresponding solutions are provided. Simulation and experimental results show that the nominal HDS can be controlled to be within 10 nm with a standard variation of 1.5 nm.

I. INTRODUCTION

The dimensions in magnetic recording components are shrinking rapidly in order to maintain continuous increase of storage density. Magnetic recording heads have critical feature sizes below 100 nm. They fly in close proximity to a recording medium at 5-15 nm fly heights using an airbearing on a 1×1 mm^2 slider surface. At these dimensions, precision metrology is a critical enabler for sustaining product quality and reliability.

To enhance magnetic recording metrology [1], we are developing an ART with the following capabilities: to write tracks on media rotating from 0 to 400 RPM; to interconnect to sliders capable of operating up to 40 GHz; to control HDS precisely for both flyable and non-flyable media; to track follow for proper reading and writing; to synchronize reading/writing with disk's rotational position; etc. Among those capabilities, HDS control is crucial because stable airbearings cannot be formed to passively maintain a constant gap at very low disk spinning speeds (<400 RPM). HDS measurement and servo control with high precision are therefore necessary.

This paper is organized as follows: Section II describes the plant setup and characterization, improvements in sensor quality and actuator dynamics, and necessary architecture modification are also presented. Section III presents the HDS control design including feedback control, repetitive control and smooth approaching. Section IV shows the experimental results. Section V concludes this paper.

II. PLANT SETUP AND CHARACTERIZATION

A photograph of the ART is shown in Fig. 1. Its architecture is depicted in [1]. A linear stage moves the bottom table and the whole platform in or out underneath a disk. The disk is mounted to the bottom of the spindle motor which is attached to a rigid frame. Three pitch/roll/Z tuning stages between the two tables control the position and orientation of the top table and hence the clamp/slider/sensor assembly

The authors are with Seagate Technology, 1251 Waterfront Place, Pittsburgh, PA 15222, USA, `xinghui.huang@seagate.com`.
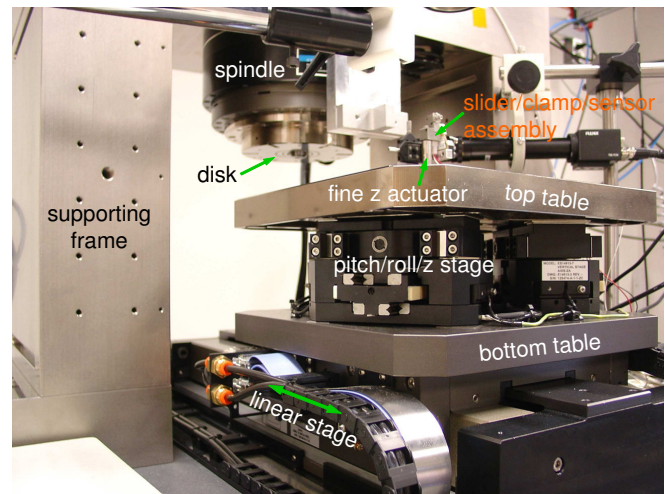
Fig. 1. Close-up of the rotary tester

on it. A fine Z piezo between the assembly and the top table generates subnanometer-precision Z motion of the slider. A fiber interferometer is mounted in the assembly to measure the slider-disk spacing for feedback control. At the desired head-media spacing level of a few nanometers, the slider orientation needs to be carefully calibrated and paralleled to avoid crashes with the disk surface.

A. Sensor Characterization

A fiber interferometer is embedded in the slider clamp to measure the HDS for feedback control by the fine Z piezo. At the targeted HDS of a few nanometers, the sensor quality plays an important role in the final performance of the servo system. Characterization of sensor noise is therefore necessary and even critical. To this end, a series of measurements are taken at various sensor gains. By comparing their frequency spectra, sensor noise is extracted from the real vibration signal, as illustrated in Fig 2. The sensor noise spectra are shown in Fig. 3.
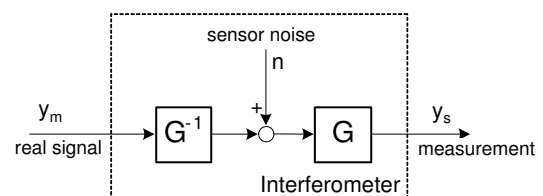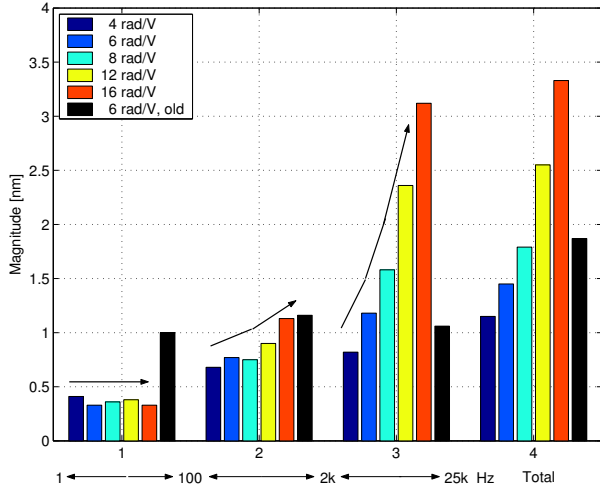

Fig. 2. Characterization of sensor noise

Fig. 3. Sensor noise characterization. Different colors represent measurements using different sensor gain G. In each frequency bin, stronger correlation between signal level and sensor gain implies higher level of internal electric noise.

Fig. 4. Lowpass filtering effect at cutoff frequency 10 kHz. The real signal level is well below 1 nm 1σ.

In Fig. 3, the frequency domain is divided into three bins as shown below the X axis. For comparison, the measurement result at a gain of 6 rad/V taken a year ago is also presented. Roughly, low frequency mechanical vibration below 100 Hz (bin 1) can be compensated for by the servo system; middle frequency noise and vibration (bin 2) are beyond the system's control bandwidth and may be amplified; high frequency electric noise above 2 kHz (bin 3) is beyond the actuator's dynamics range and does not affect the head motion.

Some conclusions can be drawn from Fig. 3. The noise levels in bin 3 show strong positive dependency on the sensor gains, implying that the internal noise dominates the sensor output at high frequency above 2 kHz. In bin 2, the similar but weaker dependency implies that there is still some gain-dependent internal electric noise in that frequency range. The actual vibration signal level in bin 2 may thus be as low as 0.5 nm. No dependency is observed in bin 1, implying that it consists of mostly real signal. Combining the components in bins 1 and 2, the total real signal level is estimated to be about $\sqrt{0.4^2 + 0.5^2} = 0.64$ nm 1σ.

Since the majority of the sensor noise is in the high frequency range beyond the servo bandwidth, it is desirable to filter them out before using this signal for control. This lowpass filtering also provides necessary anti-aliasing. An analog 4th-order 10 kHz lowpass Bessel filter is used to filter the raw measured data. Fig. 4 shows the filtering effect. It is noted that this lowpass filter does not remove the sensor noise completely. The noise in the middle frequency range from 100 Hz to 10 kHz still dominates the filtered signal due to the filter's relatively high cutoff frequency. The actual vibration component in the filtered signal should be well below 1 nm 1σ. The phase delay resulting from lowpass filtering will be included in the plant dynamics during system identification.
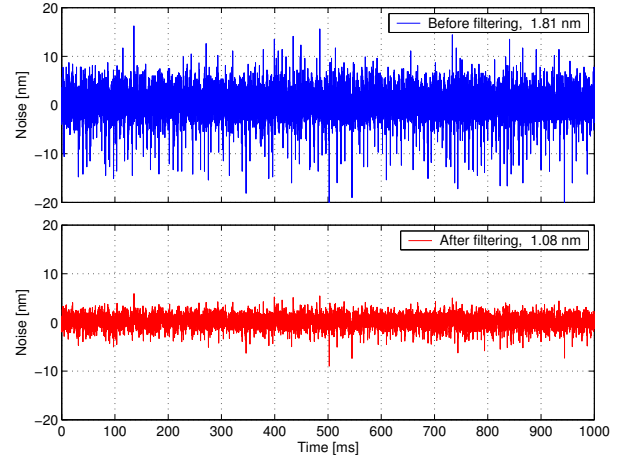
B. Uncollocated Measurement

The control system is intended to maintain the *disk-head* gap at a constant level. Ideally this gap is directly measured and used for feedback control. However, it is not feasible to install a gap sensor (interferometer) exactly at the head location. Instead, a sensor can only be put beside the slider as closely as possible as shown in Fig. 5. If only one sensor is used, serious impacts on the servo system will result.

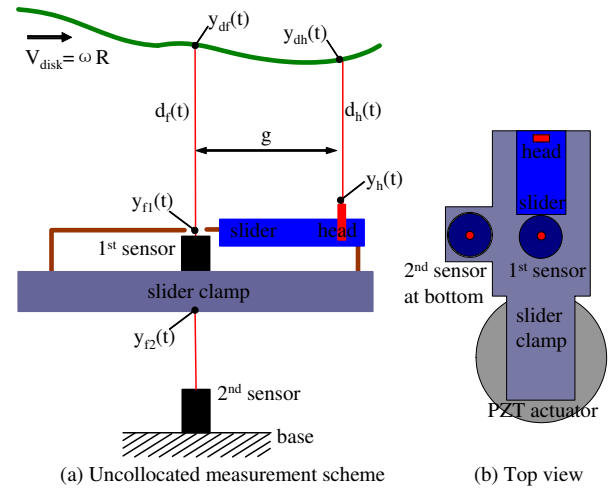(a) Uncollocated measurement scheme   (b) Top view

Fig. 5. Schematic open-loop measurement

In fig. 5, the gap g between the locations of the fiber and the head cannot be made zero and is mainly limited by the length of the slider. The consequence is that the measured disk-fiber gap $d_{\mathrm{f}}(t)$ cannot be used to control the disk-head gap $d_{\mathrm{h}}(t)$. At very low disk spinning speeds like a few revolutions per second, it is reasonable to assume that the disk profile is repeatable, then

$$y_{\mathrm{dh}}(t) = y_{\mathrm{df}}(t - \Delta). \tag{1}$$

where

$$\Delta := \frac{g}{V_{\mathrm{disk}}} = \frac{g}{\omega R}, \tag{2}$$

in which ω is the disk angular speed, and R is the radius of the head and the first fiber interferometer.

It is also reasonable to assume that the slider-clamp assembly is a rigid body and only vertical Z motion is generated by the PZT actuator. Then the three locations on the assembly, $y_{f1}(t)$, $y_{f2}(t)$ and $y_h(t)$, only differ by certain amounts of height, and they can be assumed to be the same without loss of generality. Then the disk-head gap is derived to be

$$
\begin{aligned}
d_h(t) &= y_{dh}(t) - y_h(t) \\
&= y_{df}(t - \Delta) - y_h(t) \\
&= y_{df}(t - \Delta) - y_{f1}(t) \\
&\neq y_{df}(t - \Delta) - y_{f1}(t - \Delta) = d_f(t - \Delta).
\end{aligned}
\tag{3}
$$

The above inequality results from the fact that the slider-clamp assembly is servo controlled and hence is time-varying. It is then concluded that the disk-fiber gap measurement, $d_f(t)$, alone cannot realize disk-head gap control.

A solution to this problem is to attach another fiber interferometer to the mount base and measure the absolute height position, $y_{f2}(t)$, of the clamp assembly, as shown in Fig. 5. Then we have

$$
\begin{aligned}
d_h(t) &= y_{dh}(t) - y_h(t) \\
&= y_{df}(t - \Delta) - y_h(t) \\
&= d_f(t - \Delta) + y_{f2}(t - \Delta) - y_{f2}(t),
\end{aligned}
\tag{4}
$$

in which $d_f(t - \Delta)$ is measured by the first sensor, and $y_{f2}(t-\Delta)$ and $y_{f2}(t)$ are measured by the second sensor. This configuration ensures that the disk-head gap can be estimated in real time based on the repeatability assumption of the disk profile.

To implement this sensing scheme, the disk rotating speed ω, the head/fiber radius R, and the disk-fiber gap g should be measured in order to derive the time advance Δ as shown in Eq. 2.

C. Plant Characterization and Modeling

Curve fitting and state-space system identification are conducted based on the measured plant response. The input excitation signal is a 0.1 V sweepsine up to 3 kHz with a sampling rate of 50 kHz. Fig. 6 shows the measured and identified plants. Three plant modes are identified: the major Z mode of the PZT actuator at 1300 Hz, the bending mode at 500 Hz of the spindle-supporting beam above the slider, and the PZT bending mode at 210 Hz. It is unexpected that the beam's bending mode can be excited by the PZT actuator since there is a long path for the excitation force to transmit from the PZT to the above spindle motor. The PZT bending mode is due to the center-of-mass misalignment between the clamp-slider assembly and the PZT actuator.

The open-loop bandwidth is mainly limited by the major actuator resonance mode around 1.3 kHz. Those modes at higher frequencies than the major mode are therefore not modeled for control design.
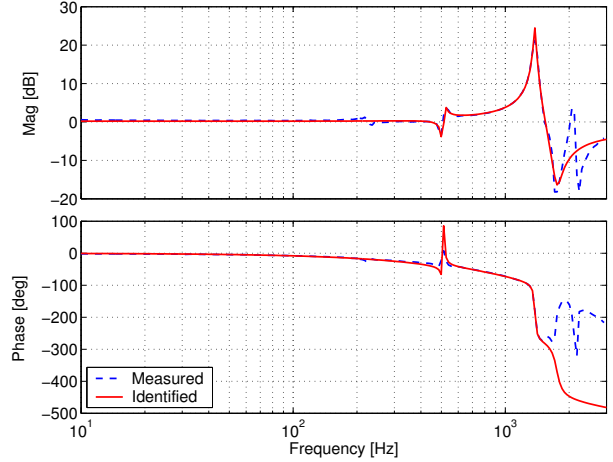

Fig. 6. Plant identification

III. CONTROL DESIGN

The identified plant model is discretized at 50 kHz. Control design is then conducted for the discrete plant model using the estimated disk-head gap. A feedback controller is first designed for real-time error compensation. For further performance improvement, an add-on repetitive controller is designed and implemented to cancel most repeatable disk profile variations. A smooth reference curve is introduced following which the head can approach the disk smoothly without generating large transient responses and overshoots.

A. Feedback Control

The feedback control design is based on classical phase lead/lag techniques for adequate gain and phase margins and integral action for sufficient gain at low frequencies. A notch filter is used to suppress the effect of the major Z mode at 1.3 kHz. Because of this mode, the actuator bandwidth has to be set around 200 Hz for stability. The continuous controller has the following form:

$$
K_{fb}(s) = k K_{int} K_{lag} K_{lead} K_{lowpass},
\tag{5}
$$

and $k = 20$, $K_{int} = \frac{1}{s}$,

$$
K_{lag} = \frac{s + 20 \cdot 2\pi}{s + 0.1 \cdot 2\pi},
$$

$$
K_{lead} = \frac{\omega_p}{\omega_z} \cdot \frac{s^2 + 2\zeta\omega_z s + \omega_z^2}{s^2 + 2\zeta\omega_p s + \omega_p^2},
$$

$$
K_{lowpass} = \frac{10^9}{(s + 350 \cdot 2\pi)^2},
$$

where $\zeta = 1.1$, $\omega_z = 359 \cdot 2\pi$, $\omega_p = 1326 \cdot 2\pi$. K_{lag} is to boost the gain below 10 Hz, and the combination of $K_{lowpass}$ and K_{lead} is to boost the gain below 1 kHz while retaining adequate phase lead around 100 Hz. These controllers are discretized using the first order hold at 50 kHz for implementation. The open-loop and closed-loop plant dynamics are shown in Fig. 7 and the closed-loop sensitivity is shown in Fig. 8.
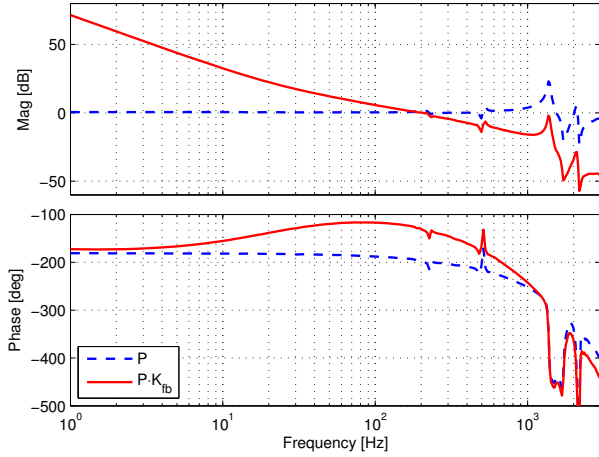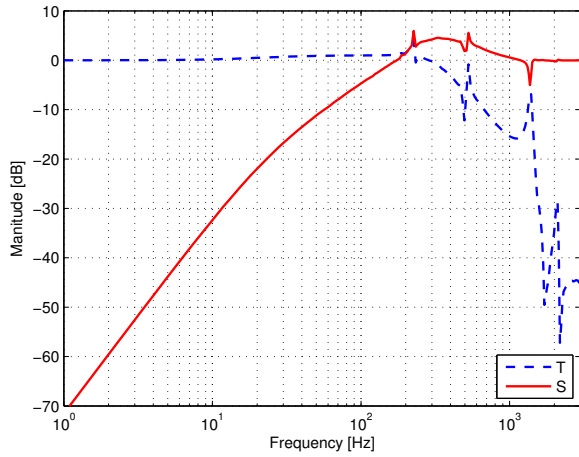
Fig. 7. Open-loop plant dynamics

Fig. 8. Closed-loop sensitivity

B. Repetitive Control

At very low disk spinning speeds, the disk profile is quite repeatable. Fig. 9 shows two disk profile trajectories when the disk rotates at 1 rev/sec. The variation between them is 3.05 nm 1σ. Assume the signal level of static measurement is 1.8 nm 1σ (the total signal level at 8 rad/V in Fig. 3), then the profile variation with respect to its nominal trajectory is $\sqrt{3.05^2/2 - 1.80^2} = 1.26$ nm. At this repeatability level, compensation of repeatable disturbance is definitely helpful especially for large and sharp spikes like the two shown in Fig. 9. All other relatively mild and low-frequency profile features can be well compensated by feedback control.

Repetitive control is widely used in canceling errors that are largely periodic in time [2][3]. The repeatability of the disk profile makes repetitive control a good application in head-media spacing control. The control block diagram is shown in Fig. 10. The repetitive controller in the dashed box consists of an internal model for repetitive signals followed by a conditioning filter denoted by K_{rep}. In this study, the zero phase error tracking controller (ZPETC) [4] is used as
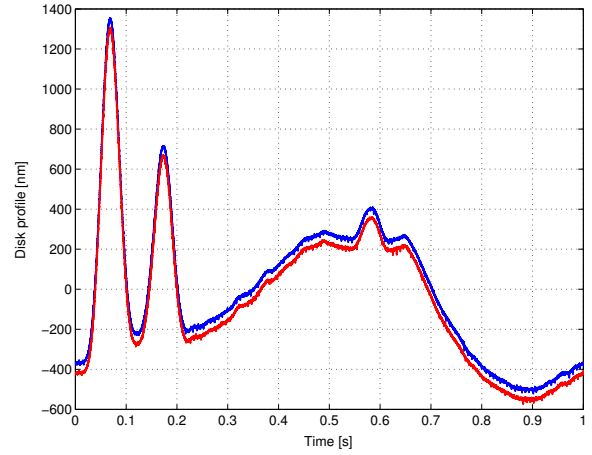

Fig. 9. Disk Z profile repeatability. Offset by 50 nm for clarity.

a conditioning filter. In that figure, y_d is the disk profile disturbance, y_{ref} is the desired disk-head spacing, n is sensing noise. An internal model loop is used to generate a repetitive control signal, which is synchronized with the disk rotating period N. K_{rep} is used to ensure stability and also for fast convergence. The internal model loop has incorporated all the delays including plant delay d_{p}, m_{u} resulting from plant's unstable zeros and m_{q} from the smoothing filter Q.

The repetitive controller is run at a lower rate than the feedback controller for memory saving. Assume the fixed number of error samples (e_r) per revolution is N_{d} and the variable disk rotating speed is T rev/sec, then the repetitive control period $N = N_{\mathrm{d}}/T$. Anti-aliasing and smoothing are performed before downsampling and upsampling respectively.
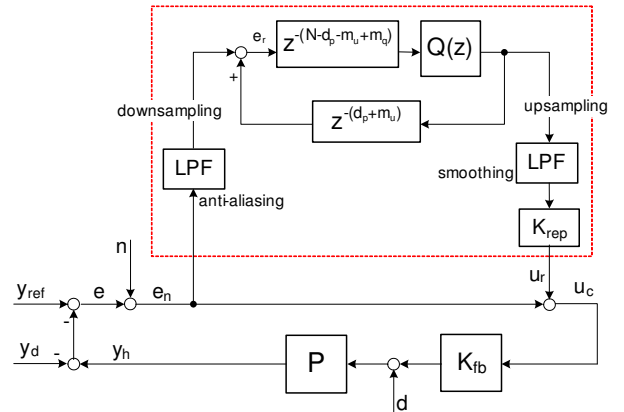

Fig. 10. Add-on repetitive control

Ideally, the conditioning filter K_{rep} is the inverse of the complementary sensitivity function of the existing feedback loop system, i.e., the transfer function from u_r to e_n in Fig. 10:

$$K_{\mathrm{rep}} \approx \left(\frac{K_{\mathrm{fb}}P}{1 + K_{\mathrm{fb}}P}\right)^{-1} = 1 + \frac{1}{K_{\mathrm{fb}}P}. \tag{6}$$

However, in most cases, exact inversion can not be realized due to unstable plant zeros. The consequence is that those unstable poles cannot be inverted and therefore extra phase delay has to be tolerated in the inversion process. ZEPTC can then be applied to maintain the phase accuracy at the cost of lower gain and hence suboptimal tracking performance [4].

Note from Fig. 8 that below 200 Hz, the transfer function of the complementary sensitivity can be well approximated as a unity constant gain, and K_{rep} may just take the inverse of that gain. This approximation is consistent with the idea that repetitive control is intended to compensate for relatively low-frequency but high-magnitude profile spikes. In Fig. 10, $Q(z, z^{-1})$ is a moving average filter having zero-phase characteristics:

$$Q(z, z^{-1}) = \frac{z + 2 + z^{-1}}{4}. \tag{7}$$

For causal implementation, its one-step advance is incorporated into the internal model loop.

C. Smooth Approaching

An procedure is needed to initialize the head-media spacing control. A straightforward one is as follows. First close the servo loop at a large nominal gap, then implement repetitive control. After the error converges, move the head smoothly to the media for a smaller desired gap. Smooth approaching is therefore necessary especially when the gap is already in the range of a few nanometers. Here, a smooth curve called minimum jerk (derivative of acceleration) trajectory is used for smooth approaching [5]:

$$y_{\mathrm{ref}}(t) = 6\left(\frac{t}{T}\right)^5 - 15\left(\frac{t}{T}\right)^4 + 10\left(\frac{t}{T}\right)^3, \tag{8}$$

where T is the time for smooth approaching.

IV. EXPERIMENTAL RESULTS

At present, head-disk gap control cannot been carried out because the current slider has only one interferometer attached to it and there is a horizontal gap between the fiber and the head. A new slider clamp has been fabricated and is to be mounted to accommodate a second fiber interferometer for real-time disk-head gap estimation and control. Based on the current hardware, servo control has been implemented and tested where very small disc-fiber spacing were achieved and maintained. Fig. 11 shows the experimental control results when the disk rotates at 1 Hz. Without repetitive control, the feedback system cannot track the large bumps in the disk profile. On the other hand, repetitive control can largely remove the remaining bumps in the error and make the final error flat. As stated in Section II-A, the actual gap variation should be well below the measured level due to dominant high frequency noise remaining in the sensor output.
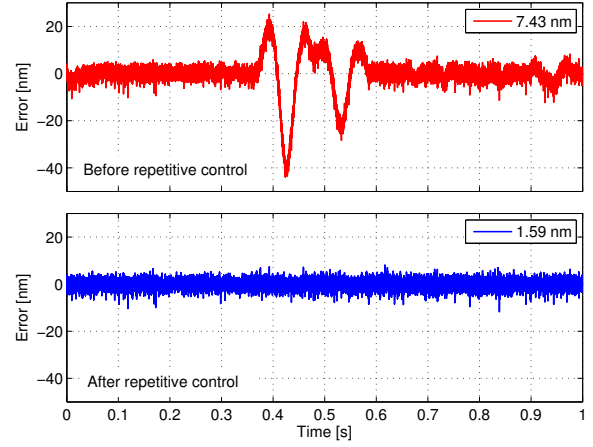

Fig. 11. Control errors before and after repetitive control. The noticeable bumps in the top figure are largely eliminated in the bottom figure.
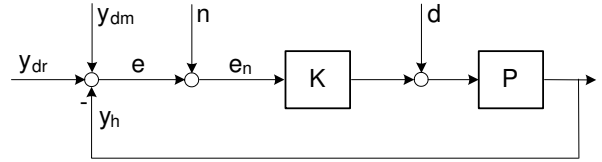

Fig. 12. Disturbances decomposition of spacing control error

V. DISTURBANCE DECOMPOSITION AND PERFORMANCE ANALYSIS

The measured head-disk spacing is always contaminated by sensor noise. At the spacing level of a few nanometers, the noise level becomes comparable to that of the real spacing. With repetitive control, the final compensation effects on repeatable and nonrepeatable disturbances are different. Therefore it makes sense to analyze the measured spacing signal in detail and estimate the actual spacing level that can be achieved by the system. To this end, the system block diagram shown in Fig. 10 is rearranged as shown in Fig. 12.

In Fig.12, the controller K includes both the feedback and repetitive parts, and the disk motion y_d has been decomposed into two parts: y_{dr} and y_{dm}. y_{dr} is the disk surface topology and is the only repeatable disturbance source; while y_{dm} is the disk motion resulting from sources like spindle motor and supporting beam modes. d represents force disturbance such as DAC quantization noise, and it is assumed to be zero in the following analysis. It is reasonable to assume that y_{dr}, y_{dm} and n are independent of each other. By estimating the three components in the frequency domain, we can extract e from e_n. The estimation procedure is as follows. Estimation of n is based on the results shown in Fig. 3 and the following relationships:
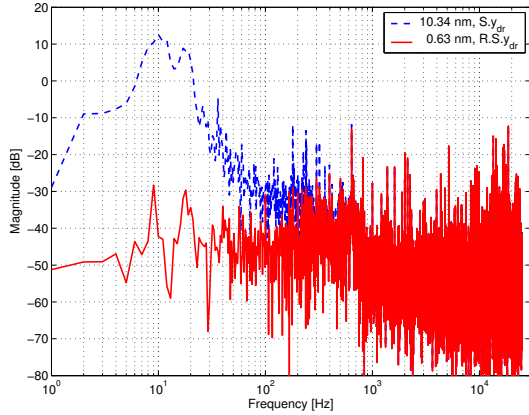
$$\begin{aligned} y_{\mathrm{s}1} &= y_{\mathrm{dm}0} + G_1 n\,, \\ y_{\mathrm{s}2} &= y_{\mathrm{dm}0} + G_2 n\,, \end{aligned} \tag{9}$$

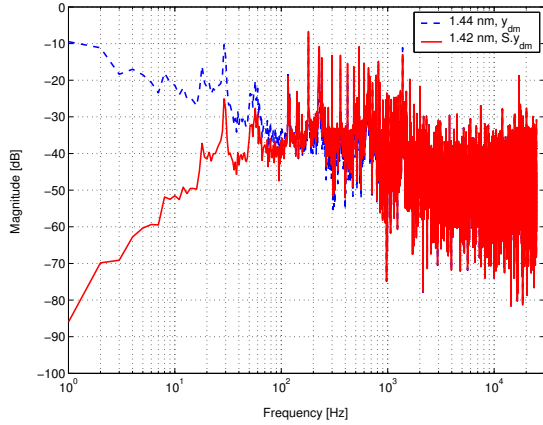where $y_{\mathrm{dm}0}$ is the nonrepeatable disk motion when it is not

rotating. Subtracting one from another yields

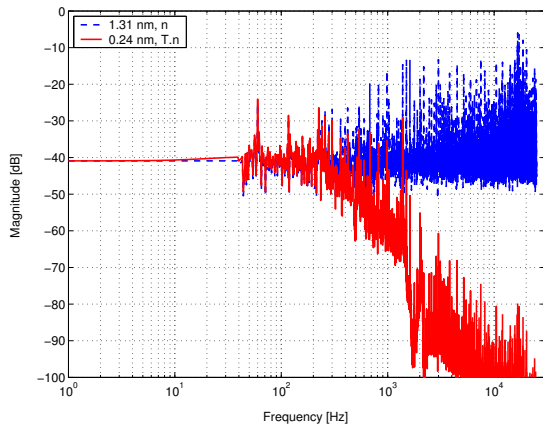$$n = \frac{y_{s1} - y_{s2}}{G_1 - G_2} . \qquad (10)$$

To estimate y_{dm} and y_{dr} at 1 Hz disk speed, the open-loop head-disk spacing is measured for a certain number of revolutions. y_{dr} is then obtained by averaging the data over

(a) Reduction of repeatable surface undulation

(b) Reduction of nonrepeatable mechanical vibration reduction

(c) Sensor noise attenuation

Fig. 13. Disturbance decomposition and performance projection. S is the sensitivity function, T is the complementary sensitivity function, and R represents the repetitive control effect.

these revolutions, and the variation after subtracting y_{dr} can be viewed as $y_{dm} + n$. It can then be further subtracted by n (Eq. 10) to extract y_{dm}. Repetitive control works mainly for repeatable y_{dr} depending on the signal-to-noise ratio. The control effect on y_{dr} is estimated by comparing the spectra of e_n before and after repetitive control.

Fig. 13 shows the results of disturbance decomposition and performance projection. From that figure, the errors can be estimated to be

$$\begin{aligned}
e &= \sqrt{0.63^2 + 1.42^2 + 0.24^2} = 1.56 \text{ nm } 1\sigma , \\
e_n &= \sqrt{0.63^2 + 1.42^2 + 1.31^2} = 2.03 \text{ nm } 1\sigma .
\end{aligned} \qquad (11)$$

The real error e is about 79% of the measured error e_n. It is also noted that the nonrepeatable disk motion y_{dm} is the biggest part in the final error e. This is mainly due to the limited closed-loop bandwidth which is currently less than 200 Hz. Further performance improvement mainly relies on improved plant dynamics and control design, and also on sensor noise reduction with higher resolution. There is some discrepancy or variation between the estimated total error (2.03 nm) and the measured error (1.59 nm in Fig. 11). Taking this into account, the real signal in the measured error is estimated to be $1.59 \times 79\% = 1.26$ nm 1σ.

VI. CONCLUSION AND FUTURE WORK

This paper has summarized the design and experimentation of head-media spacing control for an advanced rotary tester. Plant dynamics, sensing quality, disk profile repeatability, feedback and repetitive control design, smooth approaching, and issues and solutions to uncollocated measurement, are discussed in this paper. Experimental results shows that the gap control error is 1.59 nm 1σ at 1 Hz disk speed, and the estimated real error is about 1.26 nm 1σ.

A new slider clamp has been fabricated to accommodate a second fiber interferometer for real-time disk-head gap control. It is also optimized to be lighter and well-balanced so that those mechanical modes are either less excited or pushed to higher frequency. With the new clamp mounted, a second run of characterization, control design and testing is planned, and better performance is expected.

REFERENCES

[1] T. Crawford, R. van de Veerdonk, M. Bedillion, W. Koelmans, A. Langzettel, B. O'Connor, B. Novotnak, and B. Lane, "Seven-axis tester with servo-controlled flyheight for magnetic recording metrology," in *Proc. of the 21st Annual Meeting of ASPE*, Monterey, CA, November 2006.
[2] K. Chew and M. Tomizuka, "Digital control of repetitive errors in disk drive systems," *IEEE Control System Magzine*, vol. 10, pp. 16–20, 1990.
[3] M. Tomizuka and C. Kempf, "Design of discrete time repetitive controllers with applications to mechanical systems," in *Proc. 11th IFAC World Congress*, vol. 5, 1990.
[4] M. Tomizuka, "Zero-phase error tracking algorithm for digital control," *ASME J. Dynamic Systems, Measurement and Control*, vol. 109, pp. 65–68, March 1987.
[5] J. Ding, F. Marcassa, and M. Tomizuka, "Short seeking control with minimum jerk trajectories for dual actuator HDD systems," in *Proc. Amer. Control Conf.*, Boston, MA, June 2004, pp. 529–534.